



## Seasonal evolution and interannual variability of the local solar energy absorbed by the Arctic sea ice–ocean system

Donald K. Perovich,<sup>1</sup> Son V. Nghiem,<sup>2</sup> Thorsten Markus,<sup>3</sup> and Axel Schweiger<sup>4</sup>

Received 20 February 2006; revised 24 September 2006; accepted 16 October 2006; published 6 March 2007.

[1] The melt season of the Arctic sea ice cover is greatly affected by the partitioning of the incident solar radiation between reflection to the atmosphere and absorption in the ice and ocean. This partitioning exhibits a strong seasonal cycle and significant interannual variability. Data in the period 1998, 2000–2004 were analyzed in this study. Observations made during the 1997–1998 SHEBA (Surface HEat Budget of the Arctic Ocean) field experiment showed a strong seasonal dependence of the partitioning, dominated by a five-phase albedo evolution. QuikSCAT scatterometer data from the SHEBA region in 1999–2004 were used to further investigate solar partitioning in summer. The time series of scatterometer data were used to determine the onset of melt and the beginning of freezeup. This information was combined with SSM/I-derived ice concentration, TOVS-based estimates of incident solar irradiance, and SHEBA results to estimate the amount of solar energy absorbed in the ice-ocean system for these years. The average total solar energy absorbed in the ice-ocean system from April through September was  $900 \text{ MJ m}^{-2}$ . There was considerable interannual variability, with a range of 826 to  $1044 \text{ MJ m}^{-2}$ . The total amount of solar energy absorbed by the ice and ocean was strongly related to the date of melt onset, but only weakly related to the total duration of the melt season or the onset of freezeup. The timing of melt onset is significant because the incident solar energy is large and a change at this time propagates through the entire melt season, affecting the albedo every day throughout melt and freezeup.

**Citation:** Perovich, D. K., S. V. Nghiem, T. Markus, and A. Schweiger (2007), Seasonal evolution and interannual variability of the local solar energy absorbed by the Arctic sea ice–ocean system, *J. Geophys. Res.*, 112, C03005, doi:10.1029/2006JC003558.

### 1. Introduction

[2] The Arctic sea ice cover may be a sensitive indicator and a potential amplifier of climate change [Dickinson *et al.*, 1987; Moritz *et al.*, 1993; Jin *et al.*, 1994; Rind *et al.*, 1995; Battisti *et al.*, 1997; Serreze and Francis, 2005]. Numerous studies have demonstrated that the Arctic sea ice cover has been undergoing significant changes for the past few decades, with a reduction in the amount of multiyear ice [Johannessen *et al.*, 1999; Comiso, 2002], decreases in ice extent of 3% per decade [Parkinson *et al.*, 1999; Parkinson and Cavalieri, 2002], and an overall thinning of the ice [Rothrock *et al.*, 1999; Tucker *et al.*, 2001].

[3] A key element in determining the causes, and the potential implications, of these changes is understanding the interaction of solar radiation with the ice cover. Melting is

strongly affected by the partitioning of solar radiation between reflection to the atmosphere, absorption in the ice, and transmission to the ocean. This partitioning, in turn, is influenced by the timing and duration of the melt season. Of particular importance is the amount of solar energy absorbed by the ice-ocean system. This is the essence of the ice-albedo feedback, which is a powerful mechanism connecting the ice cover to the climate system.

[4] The surface heat budget of the Arctic ice cover and the ice-albedo feedback were studied in detail during the SHEBA program [Moritz *et al.*, 1993; Perovich *et al.*, 1999; Uttal *et al.*, 2002]. This program entailed a year-long field experiment plus an extensive data assimilation and modeling effort. Analysis of the field results provided considerable insights on the surface heat budget [Persson *et al.*, 2002; Andreas *et al.*, 2002], the ice mass balance [Perovich *et al.*, 2003], and the ice-albedo feedback and solar partitioning [Curry *et al.*, 2001; Perovich *et al.*, 2002a; Perovich, 2005]. The field observations made at one location for 1 year were generalized through a modeling effort that examined the underlying processes governing the surface heat budget.

[5] With only 1 year of observations, SHEBA did not investigate the interannual variability of solar partitioning. It did, however, provide a conceptual framework for such a study. In particular, during SHEBA the seasonal evolution

<sup>1</sup>Cold Regions Research and Engineering Laboratory, U.S. Army Engineer Research and Development Center, Hanover, New Hampshire, USA.

<sup>2</sup>Jet Propulsion Laboratory, California Institute of Technology, Pasadena, California, USA.

<sup>3</sup>NASA Goddard Space Flight Center, Greenbelt, Maryland, USA.

<sup>4</sup>Polar Science Center, Applied Physics Laboratory, Seattle, Washington, USA.

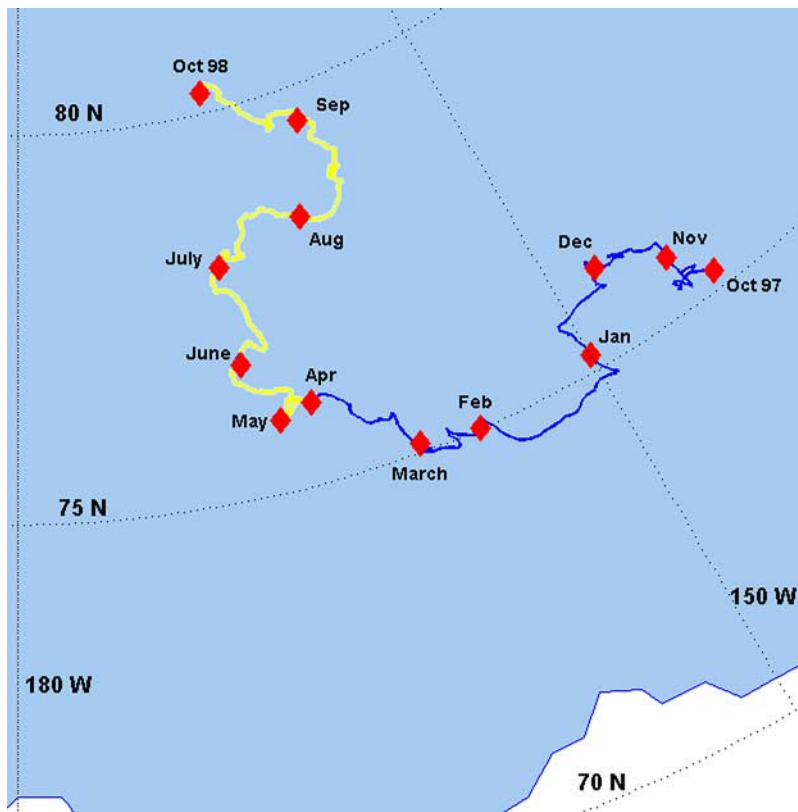


**Figure 1.** Drift of Ice Station SHEBA from October 1997 to October 1998. Our interest focuses on the period from April through September 1998 (in yellow).

of albedo was strongly influenced by the onset of melt and freezeup. For studies on the regional to Arctic Ocean scale, wide-swath satellite data are invaluable. In this study, we applied active microwave data collected by the SeaWinds scatterometer aboard the QuikSCAT satellite (denoted as QSCAT hereon) to determine the timing of melt onset and fall freezeup from 2000 through 2004 for the region where the SHEBA field experiment took place. We then combine this information with SHEBA results and Special Sensor Microwave/Imager (SSM/I) and the TIROS-N Operational Vertical Sounder (TOVS) Polar Pathfinder satellite observations to examine the interannual variability of solar partitioning.

## 2. Approach

[6] The interannual variability of the amount of solar energy absorbed in the Arctic sea ice–ocean system was investigated using a combination of SHEBA field results and QSCAT and SSM/I satellite observations. Field observations from SHEBA provided data on the temporal evolution of albedo and the incident solar radiation for 1998. The incident solar radiation for the other years was determined using data from the TOVS Polar Pathfinder satellite results. Time series of ice concentration were determined using SSM/I results, and the critical dates of onset of melt and freezeup were derived using QSCAT data. This information was used to estimate the solar energy absorbed in the ice–ocean system at the SHEBA location during April–September for 2000–2004.

[7] Five fundamental assumptions form the foundation of our analysis: (1) The general form of the albedo evolution observed during SHEBA can be applied to the same region in other years. (2) The timing of melt onset and freezeup define the seasonal albedo evolution. (3) The dates of melt onset and freezeup can be determined using QSCAT. (4) Ice concentrations can be obtained from SSM/I. (5) The downwelling solar irradiance can be adequately determined using TOVS data coupled with a simple parameterization.

### 2.1. SHEBA Observations

[8] The year-long SHEBA field experiment was conducted from October 1997 to October 1998 [Perovich *et al.*, 1999; Uttal *et al.*, 2002]. During this time, the ice station drifted over 1800 km from 75°N and 140°W to 81°N and 170°W (Figure 1). Complete time series measurements were made of both the surface heat budget and the ice mass balance. The observations included the radiative, turbulent, and conductive heat fluxes, as well as the ice growth and decay. This study focuses on the period from April through September 1998, when the input of solar radiation was a significant component of the surface heat budget.

[9] When examining solar partitioning, the first step is to determine the incident solar irradiance. Observations of the daily incident solar energy made by the SHEBA Project Office (R. E. Moritz, personal communication, 2001; <http://www.crrel.usace.army.mil/sid/perovich/SHEBAice/index.htm>) are presented in Figure 2. The seasonal cycle of solar irradiance attributable to changes in solar incident angle was evident, with values increasing from April to a

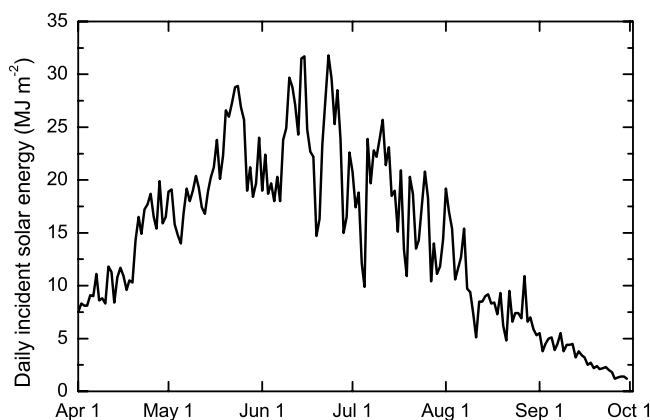


**Figure 2.** Daily incident solar energy measured at Ice Station SHEBA.

peak in June, then declining afterward. There were also rapid day-to-day changes of more than a factor of 2, ascribable to the effects of cloud cover.

[10] The key issue is determining the areally averaged albedo, the fraction of the incident energy reflected by the ice cover. Unfortunately, owing to the pervasive summer cloud cover, this quantity typically cannot be continuously monitored directly by satellite multispectral sensors. However, the areally average albedo can be estimated by combining the albedo values of the various surface types present, weighted by the relative area of each type. The surface can be simplified and considered as a combination of open water and sea ice,

$$\bar{\alpha}(t) = \alpha_{IC}(t)A_{IC}(t) + \alpha_l(t)A_l(t), \quad (1)$$

where  $\bar{\alpha}$  is the areally averaged albedo,  $\alpha$  is the albedo,  $A$  is the areal fraction, and the subscripts denote the ice cover ( $IC$ ) and leads ( $l$ ). The ice cover can be further separated into a composite of snow-covered ice, bare ice, and ponded ice. The time-dependent, areally averaged albedo is

$$\bar{\alpha}(t) = \alpha_s(t)A_s(t) + \alpha_i(t)A_i(t) + \alpha_p(t)A_p(t) + \alpha_l(t)A_l(t), \quad (2)$$

where  $t$  is time and the subscripts denote snow ( $s$ ), bare ice ( $i$ ), ponds ( $p$ ), and leads ( $l$ ). The dependence of albedo on thickness is not considered, since the focus is on ice thicker than 0.5 m. To evaluate equation (2), the time series of albedos and areal fractions of the individual components must be known. During SHEBA, a complete time series of the albedo evolution of open water [Pegau and Paulson, 2001] and of the different ice types was obtained [Perovich *et al.*, 2002a], as well as the areal fractions [Perovich *et al.*, 2002b]. All of the input parameters in equations (1) and (2) were measured during the SHEBA field experiment. The time series of the ice cover albedo evolution ( $\alpha_{IC}$ ) is plotted in Figure 3. Analyzing these results, Perovich *et al.* [2002a] determined that the evolution of areally averaged albedo had five distinct phases: dry snow, melting snow, pond formation, pond evolution, and fall freezeup. They deduced that, while the timing and amplitude of the albedo evolution might depend on location and year, the general form would be similar. Determining the timing of the phases is critical to correctly representing the albedo.

[11] The SHEBA observations provide the basis for determining the time dependence of the albedos and relative areas of the surface types. Using these findings, we derived general expressions for the five phases of the ice cover albedo ( $\alpha_{IC}$ ). This implicitly assumes that, while the duration and the timing of the melt season may vary from year to

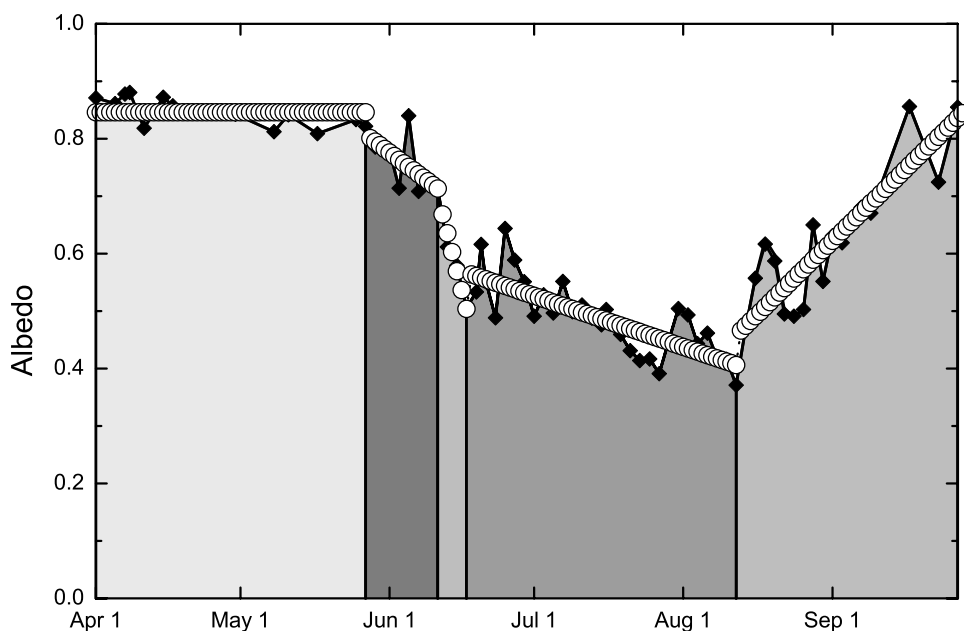


**Figure 3.** Evolution of area-averaged albedos measured during the SHEBA field experiment. There were five distinct phases as denoted by the shaded regions: dry snow, melting snow, pond formation, pond evolution, and fall freezeup [Perovich *et al.*, 2002a, 2002b]. The open circles are albedos computed using the Table 1 relationships.

**Table 1.** Best Fit Parameters for Linear Fit of the Five Phases of Albedo Evolution<sup>a</sup>

Phase	Start	End	Assumption	$a$	$b$	SHEBA
1, dry snow	4/1/1998	5/27/1998	constant value	0.846	0	
2, melting snow	5/27/1998	6/11/1998	linear decrease	0.8075	-0.00627	5/27 is day 0
3, pond formation	6/11/1998	6/17/1998	linear decrease	0.7015	-0.03298	6/11 is day 0
4, pond evolution	6/17/1998	8/12/1998	linear decrease	0.5668	-0.00287	6/17 is day 0
5, freezeup	8/12/1998	9/27/1998	linear increase	0.458	0.008217	8/12 is day 0

<sup>a</sup>Linear fit,  $\alpha_{IC}(t) = a + bt$ ;  $t$ , time in units of days; dates, m/dd/yyyy.

year, the characteristics of the albedo evolution were similar to the SHEBA site. It is possible for an exceptionally short melt season, all of the phases might not occur. For example, observations from the North Pole Environmental Observatory [Morison *et al.*, 2002] have shown summers when all the snow did not melt. Still, even in this case, the general form of the albedo evolution was valid, only the sequence was dry snow, wet snow, freezeup.

[12] We have a good understanding of the albedos of dry snow, wet snow, bare ice, and leads and their temporal dependence. There is some uncertainty about the evolution of pond albedo and pond fraction. The five phases of albedo were generalized from the SHEBA year by a linear fit for each phase using  $\alpha_{IC} = a + bt$ , where  $t$  is time in days with respect to the start time of that particular phase. Derived from the SHEBA data, the constants  $a$  and  $b$  are summarized in Table 1. These linear fits consider temporal changes in both the albedo and the melt pond fraction.

[13] To test the validity of the fitting procedures, values calculated for the 1998 SHEBA conditions were compared to the observed albedos (Figure 3). A qualitative examination of Figure 3 shows that, while observed values fluctuate above and below the linear fits, there was a good overall agreement between observed and calculated albedos. More formally, the albedo time series was combined with the observed incident solar energy (Figure 2) and equation (2) to compute the integrated solar energy absorbed to the ice cover from 1 April through 30 September. The total solar energy absorbed was  $959 \text{ MJ m}^{-2}$  using the observed albedos and  $953 \text{ MJ m}^{-2}$  for the calculated, giving a difference of only 0.6%. This is a best-case scenario, as the timing of the albedo phases is known. It does, however, demonstrate the minimal impact of smoothing the albedo fluctuations with linear fits.

[14] The calculated albedo curve has two discontinuous jumps: one at the transition between pond formation and pond evolution and the other between pond evolution and freezeup. Numerically, these discontinuities resulted from independently computing the linear relationships describing the albedo evolution for each of the five phases. However, there is a physical basis for these jumps. The albedo increase at the beginning of the pond evolution period is attributable to pond drainage and a rapid decrease in pond area [Perovich *et al.*, 2002b]. Fall freezeup is heralded by surface freezing and a light dusting of snow, resulting in a sharp increase in albedo.

## 2.2. QuikSCAT Analysis

[15] To apply the Table 1 SHEBA albedo results to other years, it is necessary to determine the timing of the transitions: in particular the dates of the onset of melt and freezeup. The onset of melt date was determined by ana-

lyzing QSCAT data along the drift positions of SHEBA. This was done by selecting ocean regions covering all SHEBA drift locations and evenly assigning centers of circular station areas (CSA) with a 25-km radius surrounding the SHEBA regions. We extracted long-term (>5 years) time series QSCAT data within each CSA, including horizontal and vertical polarization backscatter data along ascending and descending satellite passes. QSCAT results indicate that the onsets of melt and freezeup occur concurrently over length scales of hundreds of kilometers, so the precise location of the CSA is not critical. Figure 4 presents an example of the QSCAT time series signatures (Figure 4, first and second rows) at the CSA N00920 located at  $77.57^\circ\text{N}$  and  $168.12^\circ\text{W}$  near the SHEBA location on the summer solstice date (22 June). The vertical lines in Figure 4 indicate melt onset dates (red lines) and freezeup dates (blue lines) over 5 years from 1999 to 2004.

[16] Melt on the sea ice surface was identified using the diurnal approach [Nghiem *et al.*, 2001; Nghiem and Neumann, 2002]. This approach is based on differences (>1 dB) in backscatter data collected in the same day along an ascending orbit (about 6:20 am local time) and a descending orbit (about 6:20 pm) caused by different wetness values in the snow and sea ice surface layer. To match the SHEBA case, we use QSCAT results in the CSA nearest to the SHEBA melt onset location to obtain melt onset dates and in the CSA nearest to the SHEBA freezeup location to obtain freezeup dates in 2000–2004. From these dates, we can determine the melt duration for each year. Table 2 lists QSCAT results for the melt timing and duration for 2000–2004 together with SHEBA results for 1998.

[17] Surface air temperature (SAT) has been used to investigate the long-term melt climatology of Arctic sea ice [Rigor *et al.*, 2000]. However, SAT, estimated from a combination of point measurements collected by a limited number of buoys and of numerical analyses, has a large uncertainty, especially since a small fraction of a degree around the melting point is the difference between melting or freezing conditions. At locations further away from buoys (100 km), the difference between melt onset detected by radar and SAT melt date can be more than 2 weeks [Kwok *et al.*, 2003]. The QSCAT approach detects actual melting conditions on the sea ice surface with a temporal accuracy of one day and a spatial accuracy determined by the pixel size (25 km). Moreover, QSCAT's twice a day coverage of the Arctic allows for the detection of melt onset and freezeup over the entire basin without relying on interpolation from sparse point measurements.

[18] The QSCAT data provide dates for the onset of melt and the beginning of freezeup (Table 2), but not the timing of all five phases, which will require the development of more advanced and complex scatterometer algorithms in the

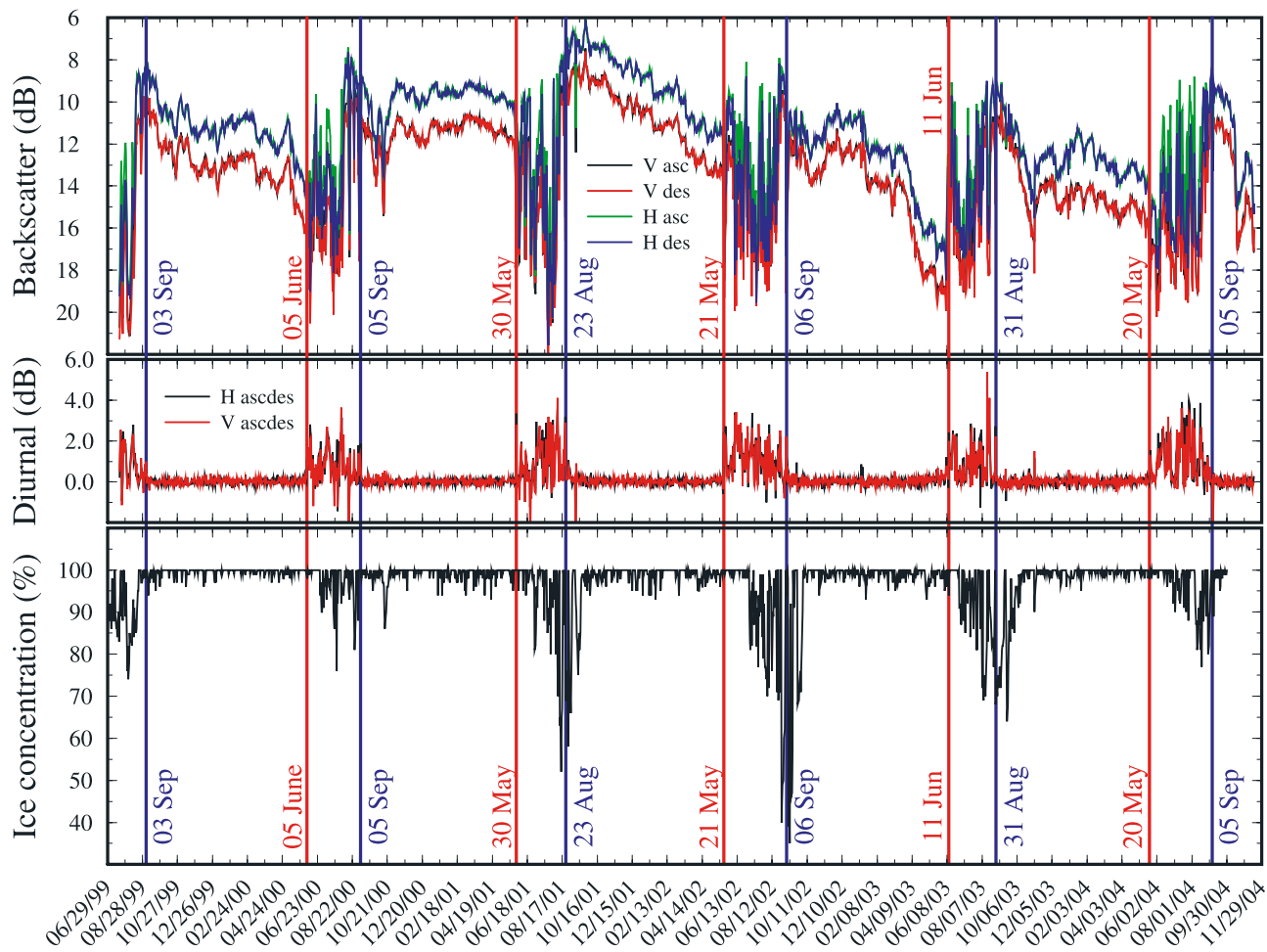


**Figure 4.** A time series of QSCAT and NT2 results from 1999 to 2004 at the CSA N00920. (top) Ascending (asc) and descending (des), horizontal (H) and vertical (V) polarization backscatter; (middle) for diurnal backscatter differences; and (bottom) NT2 ice concentration.

future. Because of this, the following assumptions are made, on the basis of the SHEBA observations, concerning the timing of the five phases.

[19] 1. For dry snow, an albedo of 0.85 is assumed until QSCAT detects melt.

[20] 2. For wet snow, once melt begins there is a fixed 15-day period of melting snow with a linearly decreasing albedo (0.801 to 0.713).

[21] 3. For pond formation, a fixed 6-day period with a linearly decreasing albedo (0.669 to 0.504).

[22] 4. For pond evolution, the remainder of the melt season with a linearly decreasing albedo. Note that the

length of this segment varies depending on the length of the melt season. Also the minimum albedo allowed during this period is 0.2.

[23] 5. For fall freezeup, this period begins when QSCAT detects freezeup. The albedo linearly increases until 30 September (end of period of interest), or until it reaches the cold snow value of 0.85.

### 2.3. Incident Solar Energy

[24] To obtain downwelling shortwave radiative fluxes varying through time and space, we combine satellite-observed cloud fraction, climatological values of surface albedo, and an “effective” optical depth. Radiative transfer

**Table 2.** Melt-Season Timing and Length for 1998, 2000–2004 Determined for the Site of Ice Station SHEBA<sup>a</sup>

	1998	2000	2001	2002	2003	2004
Melt onset	27 May	5 June	6 June	21 May	11 June	21 May
Freezeup	12 Aug	8 Aug	24 Aug	9 Sept	31 Aug	7 Sep
Melt duration, days	77	64	79	111	81	109
Total solar incident energy, MJ m <sup>-2</sup>	2644	2901	2762	2778	2688	2822
Total solar energy absorbed, MJ m <sup>-2</sup>	940	929	901	1102	849	1113
Percent deposited in ice and ocean	36%	32%	32%	40%	32%	40%
Relative contribution (ice:ocean)	(89:11)	(94:6)	(92:8)	(91:9)	(88:12)	(96:4)

<sup>a</sup>For each year, date of melt onset, date of first freezeup, melt season duration, and total solar energy absorbed are listed.

is parameterized according to *Shine* [1984]. This parameterization is highly accurate when compared to radiative transfer calculations over arctic surfaces [*Key et al.*, 1996] and requires as inputs cloud fraction, cloud optical depth, and broad-band surface albedo. The difficulty here is how to obtain these inputs. Spatially and temporally varying cloud fraction is available from satellite. Here we use daily cloud fractions from the TOVS Polar Pathfinder Project (Path-P) [*Schweiger*, 2004; *Schweiger et al.*, 2002], which have been validated against surface observations on sea ice [*Schweiger*, 2004; *Schweiger et al.*, 2002]. Following convention surface albedo measurements from the North Pole drifting station record (1956–1991) are averaged to compute daily climatological values for use as input to the parameterization. The remaining input, cloud optical depth, is not a readily available parameter. We therefore compute it by solving the *Shine* parameterization for optical depth at locations where surface observations of downwelling shortwave are available (inputs: satellite cloud fraction, surface albedo, downwelling shortwave; output: optical depth). We call the resulting optical depth value an “effective optical depth” because it includes errors in measurements, climatological inputs, parameterization, and mismatches between the resolution of observations in time and space. A seasonal cycle of monthly optical depths was computed by averaging daily effective optical depths values from measurements from the Soviet North Pole station record. The approach was then validated using independent (values that did not go into the computation of effective optical depths) measurements made at the SHEBA camp. Comparison of daily averaged surface observations of shortwave (SW) fluxes with those computed with our approach yield a root-mean-square (RMS) error of  $22 \text{ W m}^{-2}$  with a mean error of  $2.5 \text{ W m}^{-2}$ .

[25] Time series of incident solar energy for all years are plotted in Figure 5a. The incident solar energy varied considerably by day and year. The total incident energy integrated from April through September had an interannual variability of a few percent and ranged from about 2600 to 2900  $\text{MJ m}^{-2}$ . This variability may be due to uncertainties in estimating the incident irradiance at the surface. A close examination of Figure 5a reveals a noteworthy feature. There were a few downward excursions from the ensemble of curves for the 1998 observations. These small values were associated with periods of rain or thick clouds or heavy fog at SHEBA. There were no such excursions for the 2000–2005 calculated values. This argues that the computation method of estimating the solar energy reaching the surface does not consider, or properly represent, transient periods with heavy cloud cover.

#### 2.4. SSM/I Analysis

[26] The final term needed to evaluate Equation 2 is the ice concentration ( $A_i$ ). The NASA-Team 2 (NT2) algorithm [*Markus and Cavalieri*, 2000] was applied to SSM/I data to determine the ice concentration. NT2 total ice concentration at the CSA N00920 is plotted in Figure 4 (bottom row) together with QSCAT signatures. *Markus and Dokken* [2002] evaluated algorithm performance during the Arctic summer, showing that NT2 ice concentrations are much improved compared to previous algorithms; the complexity and heterogeneity of summertime sea ice has always been a

significant problem for passive microwave retrievals of sea ice during this season. This study has indicated that, for example, the ice concentration using the original NASA Team algorithm [*Cavalieri et al.*, 1984] shows an erroneous decrease of about 20% during the melting season, whereas the NT2 ice concentration stays higher. A comparison of summer NT2 ice concentrations with SAR data has shown negligible bias for the central Arctic and a bias of  $-5\%$  closer to the marginal sea ice zone. The error in albedo associated with a 5% error in ice concentration depends to a large extent on the stage of melt and its corresponding albedo. Assuming an albedo of 0.1 for open water, an underestimate of 5% in ice concentration translates to an error in albedo of 4.5% when the sea ice albedo is 0.8 and to an albedo error of 2.5% when the sea ice albedo is 0.2.

[27] The time series of SSM/I ice concentration were extracted along the SHEBA drift locations (unlike at the fixed CSA N00920 in Figure 4 (bottom row)). The results are presented in Figure 5c for 1998 and 2000–2004. In all years, there is a general seasonal cycle of a sea ice cover, with little open water, during winter, with a reduction in ice concentration starting about July and minimum values in late August or September. There is considerable day-to-day variability, as well as interannual variability during the melt season. Changes in ice concentration have the greatest impact in May and June, when the incident solar energy is highest and the differences between the albedos of the snow-covered ice (0.84) and leads (0.07) are largest (ratio of 12:1). In all years, ice concentrations were large (0.95–1.00) during this period. When ice concentrations were reaching minima in August and September, the incident solar radiation has declined to about 20–30% of peak values and the albedo contrast between ice and leads was only about 5:1.

### 3. Results and Discussion

[28] The daily incident solar energy, the calculated time series of ice cover albedo evolution ( $\alpha_{IC}(t)$ ), and the cumulative solar energy absorbed by the ice-ocean system determined from equation (2) for the years 1998, 2000, 2001, 2002, 2003, and 2004 are plotted in Figure 5, together with total ice concentration along the SHEBA drift. The bars across the top of the plot denote the duration of the melt season for each of the 6 years as determined by direct observation (1998) or from QSCAT results (Table 2). The longest melt season was in 2002 and the shortest was in 2000. The incident solar energy is plotted (Figure 5a) for reference and comparison.

[29] In April and early May, the ice cover albedo and the solar energy absorbed by the ice-ocean system (including both the ice and the leads) is similar for all years (Figure 5d). In this premelt period, the albedo of the snow-covered ice was about 0.85 in all years and the only difference in daily solar energy absorbed by the ice-ocean system was attributable to small variations in the ice concentration. Since the melt onset date varies from year to year, the albedo and solar-energy-absorbed curves began to diverge in late May. The most solar energy was absorbed in June and July, when the incident solar energy was greatest and the ice albedo was decreasing. The solar energy absorbed tapers off in August and September as the incident solar

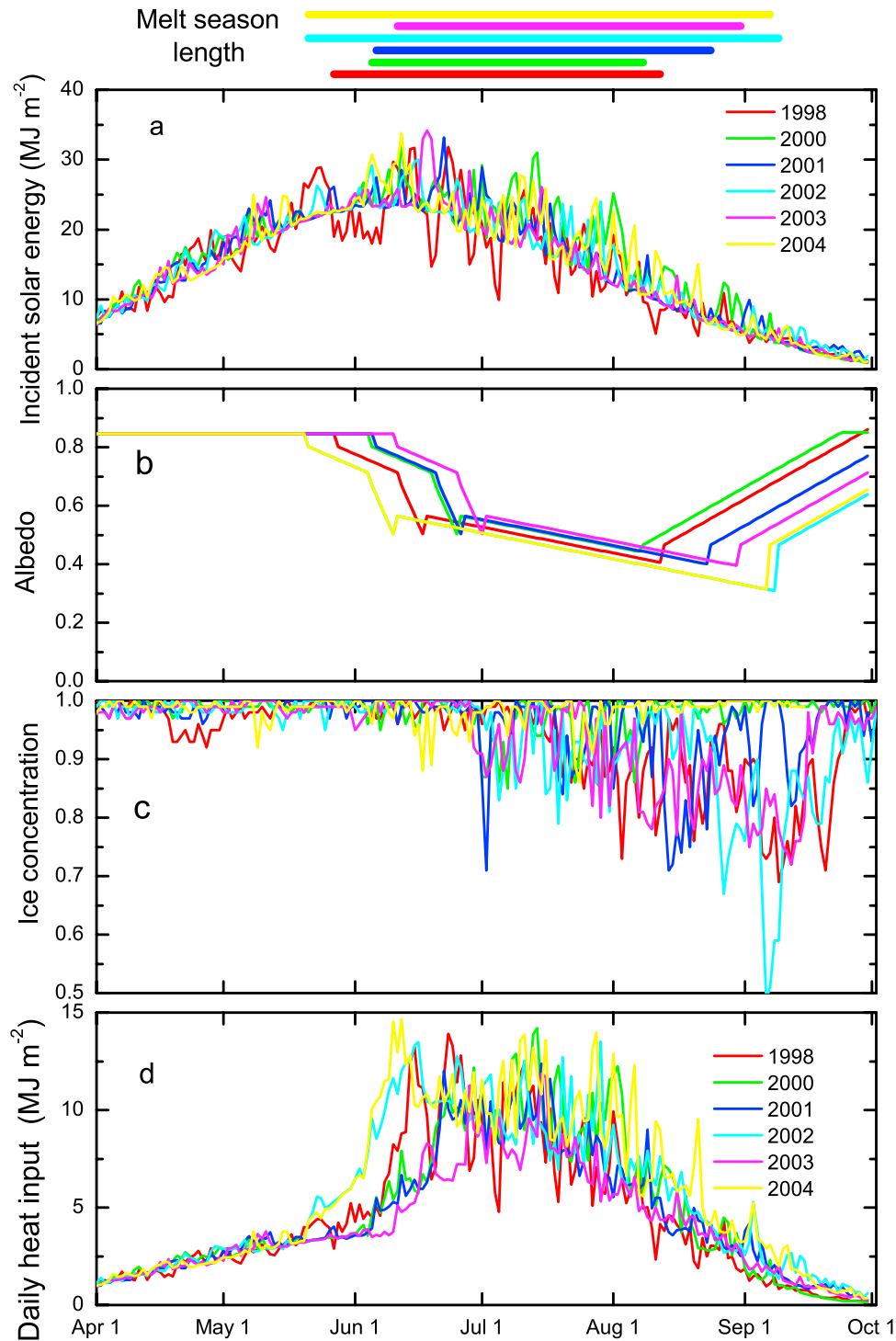


**Figure 5.** Estimates of solar energy partitioning in 1998, 2000, 2001, 2002, 2003, and 2004. The colored bars at the top of the plot denote the timing of the melt season for each year. Plotted are (a) the daily incident solar energy, (b) the calculated time series of albedo evolution ( $\alpha_{IC}(t)$ ), (c) the ice concentration, and (d) the daily solar energy absorbed by the ice-ocean system.

energy decreases and the albedo increases as freezeup progresses.

[30] Figure 6a shows the time series of integrated solar energy absorbed. The increase is slow in April and May and interannual differences are small. In June and July, both the rate that solar energy is absorbed and the interannual

variability increase. The total calculated solar energy absorbed by the ice-ocean system for each of the 6 years is reported in Table 2 and plotted in Figure 6b. The greatest total solar energy was absorbed by the ice-ocean system in 2002 and 2004. Both years had the earliest melt onset (21 May) and the longest melt duration. The 2004 melt

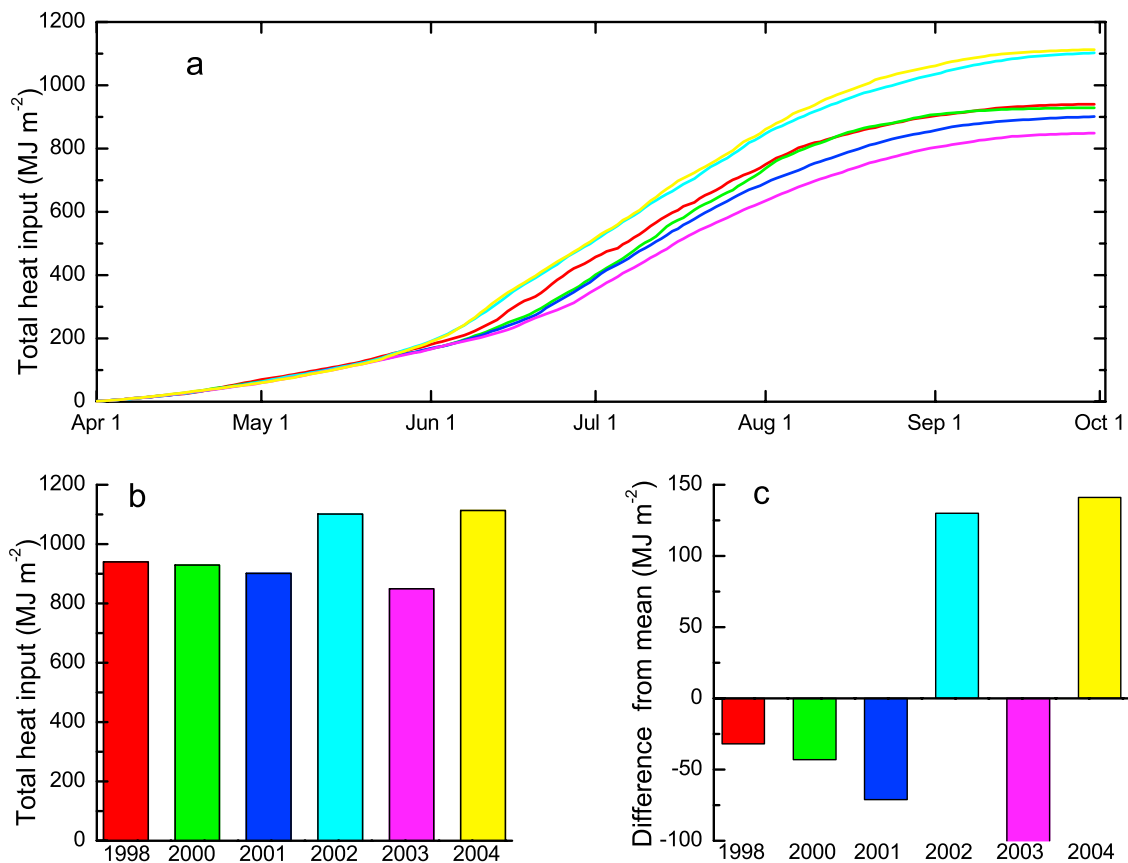


**Figure 6.** Solar energy absorbed by the ice–ocean system from April through September in 1998, 2000, 2001, 2002, 2003, and 2004 for the SHEBA location: (a) cumulative time series of absorbed total solar energy absorbed, (b) total solar energy absorbed, and (c) difference from the 5-year average.

season ended 2 days earlier than 2002, but the total incident solar energy was slightly greater in 2004. The total solar energy absorbed averaged over all years was  $970 \text{ MJ m}^{-2}$ , but there was considerable interannual variability, as evidenced by a range of 850 to  $1100 \text{ MJ m}^{-2}$  and year to year changes of  $250 \text{ MJ m}^{-2}$  (Figure 6c). As  $3 \text{ MJ m}^{-2}$  is needed to thin the ice cover by 1 cm, the range of solar energy absorbed represents potential ice thickness changes of tens of centimeters. Other terms in the surface heat budget may well counteract some of the impact of an increase in the solar energy absorbed. However, melting could also be accelerated through the ice-albedo feedback. Most of the energy input to the ice–ocean system is through the ice cover, with contributions from the ice 9 to 20 times greater than from leads.

[31] While 6 years represents only a limited sample, we can still examine the relationships between the solar energy absorbed and melt season timing and duration in a preliminary way. Scattergrams of the duration of melt, the start of melt, the start of freezeup, and the incident solar energy versus total solar energy absorbed for 1998, 2000, 2001, 2002, 2003, and 2004 are presented in Figure 7. There is a weak trend, but considerable scatter between the duration of melt and the total solar energy absorbed (linear fit  $R^2 = 0.73$ ). For example, the shortest duration had the second largest solar energy absorbed, while the second longest melt had the second smallest solar energy absorbed. Also 1998,

2001, and 2003 had melt seasons of similar length (between 77 and 81 days), but total solar energy absorbed not only varied from 849 to  $940 \text{ MJ m}^{-2}$ , but decreased with increasing melt season length. As Figure 7b indicates, the total solar energy absorbed was related to the onset of melt ( $R^2 = 0.88$ ). In general, the earlier the onset of melt was, the greater was the total solar energy absorbed. The beginning of freezeup (Figure 7c) was not strongly related to the solar energy absorbed ( $R^2 = 0.34$ ). Similarly, the solar energy absorbed was not correlated to the total incident solar energy (Figure 7d) ( $R^2 = 0.12$ ). The lack of a correlation between the incident and absorbed solar energy may seem counterintuitive, but it is a consequence of the importance of timing. Interannual differences in incident solar energy were only a few percent, much smaller than the impact caused by the changes in the albedo by an earlier start of the melt season.

[32] The relationship between the total solar energy absorbed and the dates of melt onset and freezeup is examined in more detail in Figure 8 by isolating each variable. Values of incident solar energy observed at SHEBA and ice concentrations for 1998 were used in these calculations. The melt onset curve was computed assuming a freezeup date of 15 August for all cases and then varying the date of melt onset. Similarly, the freezeup onset curve assumed that melt onset was always 1 June and varied the freezeup date. While there is some curvature and variability

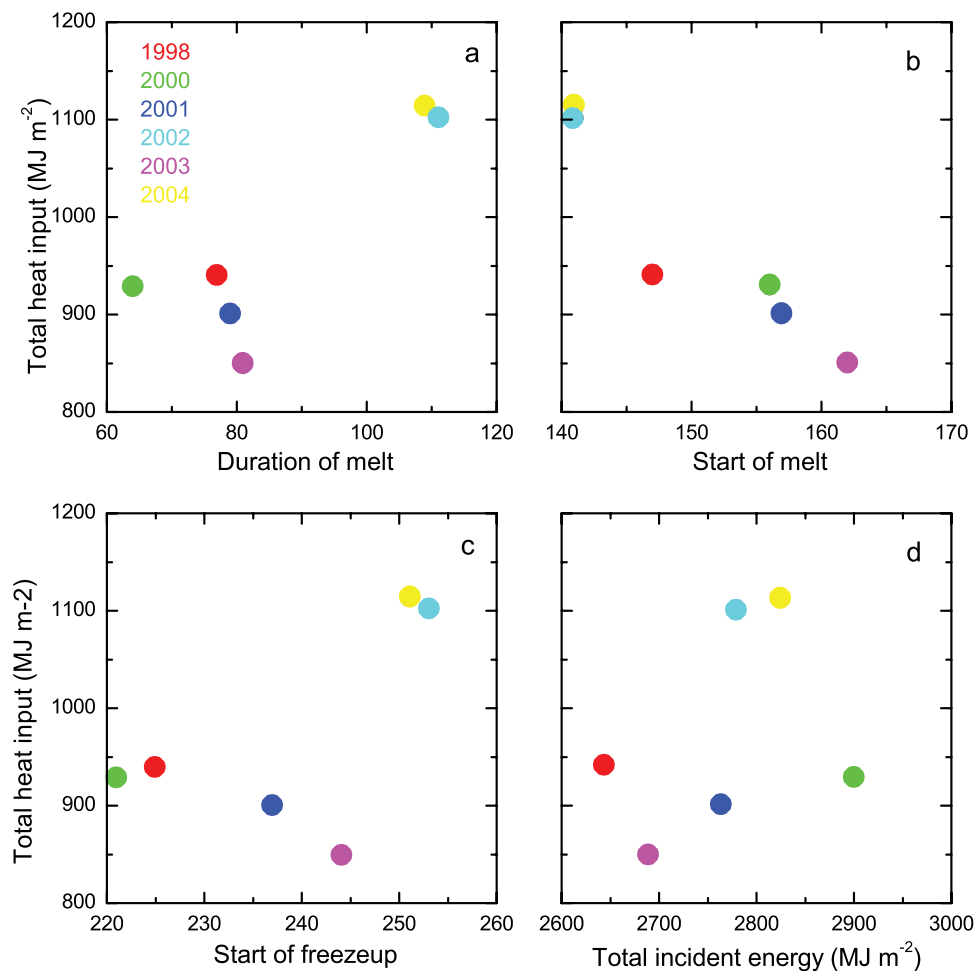


**Figure 7.** Scattergrams of (a) duration of melt, (b) start of melt, (c) start of freezeup, and (d) total incident solar energy versus total solar energy absorbed for 1998, 2000, 2001, 2002, 2003, and 2004.

in the lines, the overall shapes are roughly linear ( $R^2 = 0.99$ ). The slope of the melt onset curve is almost six times greater than that of the freezeup curve. Each day that melt starts earlier increases the cumulative solar energy absorbed by about  $8.7 \text{ MJ m}^{-2}$ , while a 1-day delay in freezeup results in an increase of only  $1.5 \text{ MJ m}^{-2}$ .

[33] The total solar energy absorbed is much more sensitive to the timing of melt onset than that of fall freezeup. There are two fundamental reasons why a day in the spring has a larger impact than a day in the fall. The first is rather obvious: The incident solar radiation is much larger in May and June than in August and September. The second is more subtle: a change in the timing of melt onset propagates through the entire melt season, affecting the albedo every day afterward. Changes in freezeup affect a much shorter period of time and consequently their impact on solar energy absorbed is less.

[34] Figure 9 displays the ice extent in the Beaufort Sea derived from a scatterometer algorithm using QSCAT data [Nghiem *et al.*, 2005] on the fall equinox date (22 September) for each of years 1999–2004 when the ice extent is close to minimal. The minimum extent is governed by a combination of ice dynamics and thermodynamics. The thermodynamic relationship is apparent: the ice retreat is greater in years when

the solar energy absorbed is above average, such as in 2002 and 2004 (Figure 9). There also is evidence that the solar energy absorbed in the summer season of one year may influence sea ice conditions in the next year. This is demonstrated in 2000 and 2003, where both years have roughly comparable, below average values of solar energy absorbed. However, 2003 followed the maximum solar energy absorbed year of 2002 and had less ice. This effect is also evident in 2000 and 2001, where two consecutive below-average years of absorbed solar energy (2000 and 2001) resulted in a southerly advance of the ice edge. In essence, the solar energy absorbed in 1 year may precondition the ice pack for the following year.

[35] This illustrates the importance of both ice thermodynamics and dynamics on ice mass balance in a freezing season affected by solar energy absorbed in the preceding summer season. This is supported by the QSCAT and SSM/I time series signatures in Figure 4 that were measured over the central location of the SHEBA region (CSA N00920). These results show: (1) higher seasonally averaged backscatter representing higher concentration or thicker and older ice, which has lower salinity and higher backscatter [Nghiem *et al.*, 1995a, 1995b], distribution in the 2000–2001 sea ice season between 5 September 2000 and 30 May

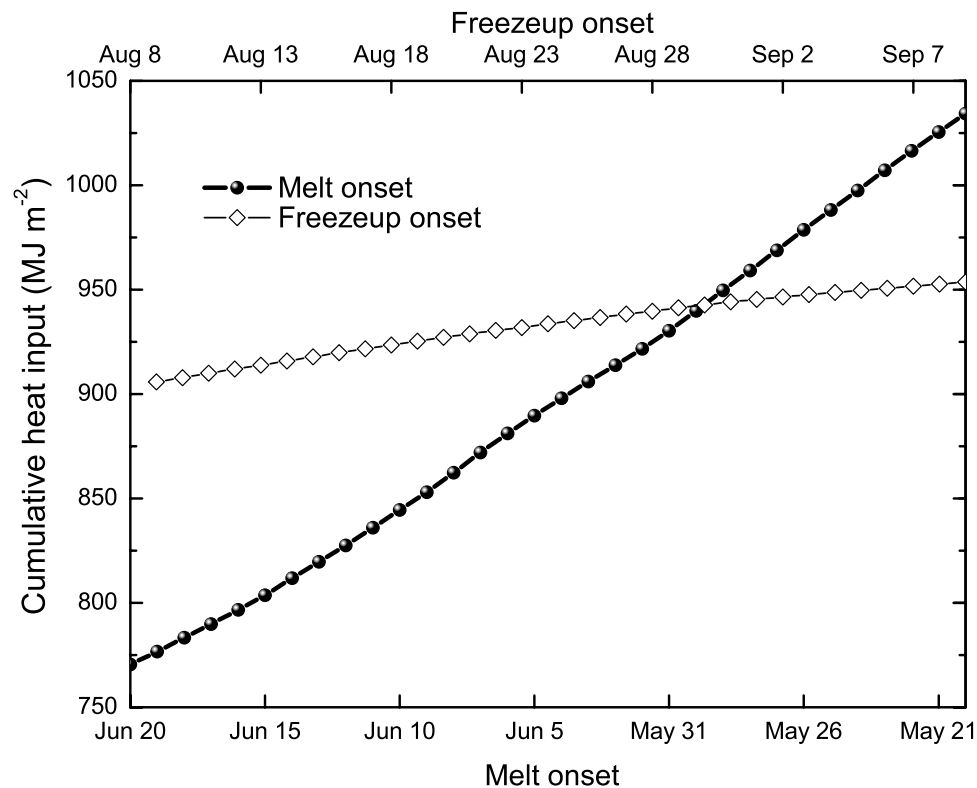


**Figure 8.** Effect of melt onset and fall freezeup dates on the total solar energy absorbed by the ice-ocean system. The melt onset curve is computed assuming a constant freezeup date of 15 August and variable dates of melt onset (bottom x axis). Similarly, the freezeup onset curve assumes a constant melt onset date of June 1 and a variable freezeup date (top x axis).

2001, following the below-average solar energy absorbed in summer 2000; (2) higher seasonal backscatter and thus more ice in the 2001–2002 sea ice season between 23 August 2001 and 21 May 2002, following another below-average solar energy absorbed in summer 2001; (3) much lower backscatter, corresponding to less ice in the 2002–2003 sea ice season between 6 September 2002 and 11 June 2003, following the largest solar energy absorbed in summer 2002; and (4) increased backscatter and thus more ice conditions in the 2003–2004 sea ice season between 31 August 2003 and 20 May 2004, following the below-average solar energy absorbed in summer 2003. Moreover, in all years, there was a general decreasing trend in backscatter (Figure 4, top row) and increasing trend in SSM/I GR (Figure 4, bottom row) before the melt onset, indicating that more FY ice was pushed into the SHEBA region owing to ice dynamics. This was most pronounced in 2003, contributing to the poleward retreat of the ice edge although the solar energy absorbed was below average. The above evidence suggests that the solar energy absorbed impacts sea ice conditions in the following season. However, other factors, such as atmospheric interactions (heat convection, cloud feedback, etc.), and ocean mixing, also contribute significantly to the overall seasonal evolution of Arctic sea ice.

[36] This relatively short 6-year data set measured at a single location is inherently limited. Thus this analysis is only a first step in the large-scale examination of the absorption of solar energy by the Arctic sea ice cover. In

other regions of the Arctic, solar energy absorbed trends may be different. For example, the ice edge advanced further south in the region near the CSA N00840 located at  $76.667^{\circ}\text{N}$  and  $155.783^{\circ}\text{E}$  (northeast of the Novosibirskiye Ostrova or the New Siberian Islands) in the East Siberian Sea in 2004 compared to 2003. QSCAT results at N00840 show an early melt onset (26 May) in 2003 and a late melt (12 June) in 2004 as opposed to the 2003 later melt and the 2004 earlier melt near the CSA N00920 in the SHEBA region. QSCAT data are available to extend this analysis to examine almost all of the Arctic Basin by applying the same techniques to determine the onset dates of melt and freezeup. To investigate both the thermodynamics and dynamics of sea ice, the entire time series of satellite data need to be analyzed for each pixel over the entire Arctic.

[37] Furthermore, other aspects of the methodology, including the basic assumptions concerning the albedo evolution, will need to be modified. While the general attributes of the albedo evolution will be present at other locations, the details will likely be different. The first albedo phase of premelt dry snow will be the same anywhere [Grenfell and Maykut, 1977; Warren, 1982]. The decrease in albedo from dry snow (0.85) to melting snow (0.70) will also be the same, but the duration of the melting snow period will probably be different. Similarly, the length of the transition period of melt pond formation will be expected to vary as a function of latitude and in different regions. For example, results from autonomous mass balance buoys [Morison et

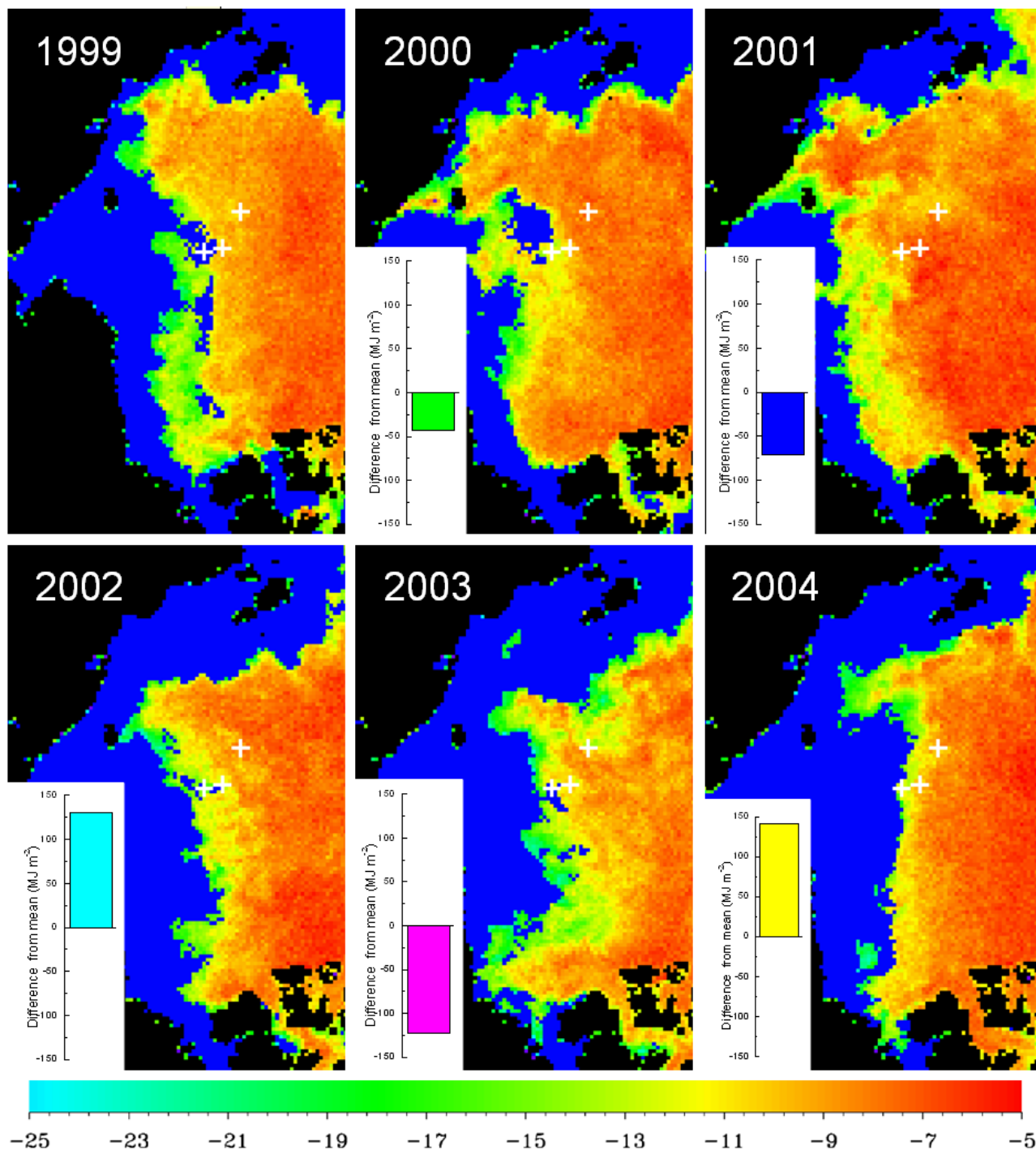


**Figure 9.** Sea ice extent on 22 September for 1999–2004. Dark blue represents open water. QSCAT forward-look horizontal-polarization backscatter in decibels is plotted over sea-ice-covered area with a color scale from light blue to red. The white plus signs represent the center locations of CSA’s N00849 (near SHEBA melt-onset location), N00920 (near SHEBA solstice location), and N00987 (near SHEBA freezeup location), respectively, from left to right. Also plotted is the deviation from the 6-year mean of the total April–September solar energy absorbed by the ice ocean system.

*al.*, 2002; Richter-Menge *et al.*, 2007] installed near the North Pole show considerable interannual variability in the length of the snowmelt and pond formation periods. In some years, there is little surface ice melt and ponds do not even form.

[38] Because of the spatial variability in the length and intensity of the albedo phases, it will also be necessary to determine the transition onset dates and areal fractions of pond formation and pond evolution. This will require the development of more advanced algorithms combining

active and passive microwave data to determine time series of pond fractions for different regions. Furthermore, cloud cover strongly influences both the shortwave and longwave radiation components of the energy balance and causes uncertainties in energy estimates. Cloud data, such as that from the International Satellite Cloud Climatology Project or ISCCP [Rossow and Duenas, 2004; Van Woert, 1999], will contribute to generating basin-wide estimates of the incident solar energy and calculating the total radiative heat budget.

#### 4. Conclusions

[39] Observations from the scatterometer on the QSCAT satellite can provide the dates of melt onset and fall freezeup. When coupled with information on ice concentration and the existing observational data set of albedo evolution, estimates of the amount of solar energy absorbed by the Arctic sea ice cover can be calculated. The solar energy absorbed by the ice and ocean displays a strong seasonal trend, with peak values occurring between mid-June and mid-July, as well as significant interannual variability. Over the 6 years studied (1998–2004), the total solar energy absorbed by the ice-ocean system ranged from 850 to 1100 MJ m<sup>-2</sup>. The solar energy absorbed depended much more strongly on the timing of the onset of melt than with the total incident solar energy. These differences in solar energy absorbed could result in interannual variations in ice ablation of tens of centimeters per year. Years with large solar energy absorbed appear to be correlated with reduced ice extent. The total solar absorbed is more strongly related to the timing of the onset of melt than to the onset of freezeup or the duration of melt. Stated simply, a day of melting in the spring has a much greater impact than a day in late summer. Each day melt starts earlier increases cumulative solar energy absorbed by about 8.7 MJ m<sup>-2</sup> (~3 cm of melt) while a 1 day delay in freezeup only increases the cumulative solar energy absorbed by about 1.5 MJ m<sup>-2</sup> (~0.5 cm of melt). This is a direct consequence of the larger values of incident solar energy in May and June and the cumulative impact over the entire melt season of a change at the beginning. The impact of date of melt onset on total solar input suggests that storms and warm air masses in late spring may have great influence by triggering the onset of melt [Bitz et al., 1996]. The next step in this effort will be to extend this analysis to the entire Arctic Basin, providing a large-scale examination of the changing solar energy absorbed by a changing ice cover and its impact on Arctic ice mass balance.

[40] **Acknowledgments.** This work was funded under NASA contracts NAG5-11800 and NNH04AA711-1. The research carried out at the Jet Propulsion Laboratory (JPL), California Institute of Technology, was supported by the National Aeronautics and Space Administration (NASA). We thank the SHEBA Project Office for the use of the incident solar irradiance data. Special thanks go to G. Neumann of JPL for QSCAT data processing.

#### References

Andreas, E. L., P. S. Guest, P. O. G. Persson, C. W. Fairall, T. W. Horst, S. R. Semmer, and R. E. Moritz (2002), Near-surface water vapor over polar sea ice is always near ice saturation, *J. Geophys. Res.*, *107*(C10), 8032, doi:10.1029/2000JC000411.

- Battisti, D. S., C. M. Bitz, and R. E. Moritz (1997), Do general circulation models underestimate the natural variability in the Arctic climate?, *J. Clim.*, *10*, 1909–1920.
- Bitz, C. M., D. S. Battisti, R. E. Moritz, and J. A. Beesley (1996), Low frequency variability in the Arctic atmosphere, sea ice, and upper ocean climate system, *J. Clim.*, *9*, 394–408.
- Cavalieri, D. J., P. Gloersen, and W. J. Campbell (1984), Determination of sea ice parameters with the NIMBUS 7 SMMR, *J. Geophys. Res.*, *89*(D4), 5355–5369.
- Comiso, J. C. (2002), A rapidly declining perennial sea ice cover in the Arctic, *Geophys. Res. Lett.*, *29*(20), 1956, doi:10.1029/2002GL015650.
- Curry, J. A., J. L. Schramm, D. K. Perovich, and J. O. Pinto (2001), Applications of SHEBA/FIRE data to evaluation of snow/ice albedo parameterizations, *J. Geophys. Res.*, *106*(D14), 15,345–15,355.
- Dickinson, R. E., G. A. Meehl, and W. M. Washington (1987), Ice-albedo feedback in a CO<sub>2</sub>-doubling simulation, *Clim. Change*, *10*, 241–248.
- Grenfell, T. C., and G. A. Maykut (1977), The optical properties of ice and snow in the Arctic Basin, *J. Glaciol.*, *18*, 445–463.
- Jin, Z., K. Stamnes, and W. F. Weeks (1994), The effect of sea ice on the solar energy budget in the atmosphere-sea ice-ocean system: A model study, *J. Geophys. Res.*, *99*(C12), 25,281–25,294.
- Johannessen, O. M., E. V. Shalina, and M. W. Miles (1999), Satellite evidence for an Arctic sea ice cover in transformation, *Science*, *286*(5446), 1937–1939.
- Key, J. R., R. A. Silcox, and R. S. Stone (1996), Evaluation of surface radiative flux parameterizations for use in sea ice models, *J. Geophys. Res.*, *101*(C2), 3839–3849.
- Kwok, R., G. F. Cunningham, and S. V. Nghiem (2003), A study of melt over the Arctic Ocean in RADARSAT synthetic aperture radar data, *J. Geophys. Res.*, *108*(C11), 3363, doi:10.1029/2002JC001363.
- Markus, T., and D. J. Cavalieri (2000), An enhancement of the NASA Team sea ice algorithm, *IEEE Trans. Geosci. Remote Sens.*, *38*(3), 1387–1398.
- Markus, T., and S. T. Dokken (2002), Evaluation of Arctic late summer passive microwave sea ice retrievals, *IEEE Trans. Geosci. Remote Sens.*, *40*(2), 348–356.
- Morison, J. A., et al. (2002), North Pole Environmental Observatory delivers early results, *Eos Trans. AGU*, *83*(33), 357, 360–361.
- Moritz, R. E., J. A. Curry, A. S. Thorndike, and N. Untersteiner (1993), SHEBA, a research program on the surface heat budget of the Arctic Ocean, *Rep. 3*, 34 pp., OAI Sci. Manage. Off., Univ. of Wash., Seattle.
- Nghiem, S. V., and G. Neumann (2002), Snow and ice in the Earth system viewed by space scatterometer observatory, *Eos Trans. AGU*, *83*(47), Fall Meet. Suppl., Abstract C72B-02.
- Nghiem, S. V., R. Kwok, S. H. Yueh, and M. R. Drinkwater (1995a), Polarimetric signature of sea ice: 1. Theoretical model, *J. Geophys. Res.*, *100*(C7), 13,665–13,679.
- Nghiem, S. V., R. Kwok, S. H. Yueh, and M. R. Drinkwater (1995b), Polarimetric signature of sea ice: 2. Experimental observations, *J. Geophys. Res.*, *100*(C7), 13,681–13,698.
- Nghiem, S. V., K. Steffen, R. Kwok, and W. Y. Tsai (2001), Detection of snowmelt regions on the Greenland ice sheet using diurnal backscatter change, *J. Glaciol.*, *47*(159), 539–547.
- Nghiem, S. V., M. L. Van Woert, and G. Neumann (2005), Rapid formation of a sea ice barrier east of Svalbard, *J. Geophys. Res.*, *110*, C11013, doi:10.1029/2004JC002654.
- Parkinson, C. L., and D. J. Cavalieri (2002), A 21 year record of Arctic sea-ice extents and their regional, seasonal and monthly variability and trends, *Ann. Glaciol.*, *34*, 441–446.
- Parkinson, C. L., D. J. Cavalieri, P. Gloersen, H. J. Zwally, and J. C. Comiso (1999), Arctic sea ice extents, areas, and trends, 1978–1996, *J. Geophys. Res.*, *104*(C9), 20,837–20,856.
- Pegau, W. S., and C. A. Paulson (2001), The albedo of Arctic leads in summer, *Ann. Glaciol.*, *33*, 221–224.
- Perovich, D. K. (2005), On the aggregate-scale partitioning of solar radiation in Arctic sea ice during the Surface Heat Budget of the Arctic Ocean (SHEBA) field experiment, *J. Geophys. Res.*, *110*, C03002, doi:10.1029/2004JC002512.
- Perovich, D. K., et al. (1999), Year on ice gives climate insights, *Eos Trans. AGU*, *80*(41), 481, 485–486.
- Perovich, D. K., T. C. Grenfell, B. Light, and P. V. Hobbs (2002a), Seasonal evolution of Arctic sea ice albedo, *J. Geophys. Res.*, *107*(C10), 8044, doi:10.1029/2000JC000438.
- Perovich, D. K., W. B. Tucker III, and K. A. Ligett (2002b), Aerial observations of the evolution of ice surface conditions during summer, *J. Geophys. Res.*, *107*(C10), 8048, doi:10.1029/2000JC000449.
- Perovich, D. K., T. C. Grenfell, J. A. Richter-Menge, B. Light, W. B. Tucker III, and H. Eicken (2003), Thin and thinner: Ice mass balance measurements during SHEBA, *J. Geophys. Res.*, *108*(C3), 8050, doi:10.1029/2001JC001079.

- Persson, P. O. G., C. W. Fairall, E. Andreas, P. Guest, and D. K. Perovich (2002), Measurements near the atmospheric surface flux group tower at SHEBA: Near-surface conditions and surface energy budget, *J. Geophys. Res.*, *107*(C10), 8045, doi:10.1029/2000JC000705.
- Richter-Menge, J. A., D. K. Perovich, B. C. Elder, K. Claffey, I. Rigor, and M. Ortmeier (2007), Ice mass balance buoys: A tool for measuring and attributing changes in the thickness of the Arctic sea ice cover, *Ann. Glaciol.*, in press.
- Rigor, I. G., R. L. Colony, and S. Martin (2000), Variations in surface air temperature observations in the Arctic, 1979–1997, *J. Clim.*, *13*, 896–914.
- Rind, D., R. Healy, C. Parkinson, and D. Martinson (1995), The role of sea ice in  $2 \times \text{CO}_2$  climate model sensitivity. Part I: The total influence of sea ice thickness and extent, *J. Clim.*, 450–463.
- Rossow, W. B., and E. N. Duenas (2004), The International Satellite Cloud Climatology Project (ISCCP) web site—An online resource for research, *Bull. Am. Meteorol. Soc.*, *85*, 167–172.
- Rothrock, D. A., Y. Yu, and G. A. Maykut (1999), Thinning of the Arctic sea ice cover, *Geophys. Res. Lett.*, *26*(23), 3469–3472.
- Schweiger, A. (2004), Seasonal changes in cloud cover over the Arctic seas from satellite and surface observations, *Geophys. Res. Lett.*, *31*, L12207, doi:10.1029/2004GL020067.
- Schweiger, A. J., R. W. Lindsay, J. A. Francis, J. Key, J. M. Intrieri, and M. D. Shupe (2002), Validation of TOVS Path-P data during SHEBA, *J. Geophys. Res.*, *107*(C10), 8041, doi:10.1029/2000JC000453.
- Serreze, M. C., and J. A. Francis (2005), The Arctic amplification debate, *Clim. Change*, *76*, 241–264, doi:10.1007/s10584-005-9017-y.
- Shine, K. P. (1984), Parameterization of the shortwave flux over high albedo surfaces as a function of cloud thickness and surface albedo, *Q. J. R. Meteorol. Soc.*, *110*(465), 747–764.
- Tucker, W. B., III, J. W. Weatherly, D. T. Eppler, L. D. Farmer, and D. L. Bentley (2001), Evidence for rapid thinning of sea ice in the western Arctic Ocean at the end of the 1980s, *Geophys. Res. Lett.*, *28*(14), 2851–2854.
- Uttal, T., et al. (2002), Surface heat budget of the Arctic Ocean, *Bull. Am. Meteorol. Soc.*, *83*, 255–275.
- Van Woert, M. L. (1999), Wintertime dynamics of the Terra Nova Bay polynya, *J. Geophys. Res.*, *104*(C4), 7753–7769.
- Warren, S. G. (1982), Optical properties of snow, *Rev. Geophys.*, *20*, 67–89.
- 
- T. Markus, NASA Goddard Space Flight Center, Code 975, Greenbelt, MD 20771, USA.
- S. V. Nghiem, Jet Propulsion Laboratory, California Institute of Technology, MS 300-235, 4800 Oak Grove Drive, Pasadena, CA 91109, USA.
- D. K. Perovich, Cold Regions Research and Engineering Laboratory, U.S. Army Engineer Research and Development Center, 72 Lyme Road, Hanover, NH 03755, USA. (donald.k.perovich@erdc.usace.army.mil)
- A. Schweiger, Polar Science Center, Applied Physics Laboratory, Seattle, WA 98195, USA.